Dalton Transactions

PAPER

View Article Online
View Journal | View Issue

Cite this: *Dalton Trans.*, 2018, **47**, 14340

Luminescent liquid crystalline hybrid materials by embedding octahedral molybdenum cluster anions with soft organic shells derived from tribenzo[18]crown-6†

Philipp Ehni,[a] Kevin Guy,[b] Max Ebert,[a] Stuart Beardsworth,[a] Korinna Bader,[a] Robert Forschner,[a] Andrea Bühlmeyer,[a] Noée Dumait,[b] Claire Roiland,[b] Yann Molard *[b] and Sabine Laschat *[a]

Received 9th August 2018,
Accepted 24th August 2018

DOI: 10.1039/c8dt03254h

rsc.li/dalton

Crown ethers and their derivatives are versatile building blocks for the design of supramolecular materials. They can be functionalized at will and are well known for their abilities to complex with alkali cations. Here, we show that emissive lanthanide free hybrid materials can be generated by using such building blocks. The organic tribenzo[18]crown-6 central core was functionalized *via* six-fold Suzuki cross-coupling as a key reaction with three *o*-terphenyl units which could be converted into their corresponding triphenylenes by the Scholl reaction, leading to novel liquid-crystalline columnar materials. Selected tribenzo[18]crown-6 *o*-terphenyls could interact with emissive ternary metal cluster compound salts to generate hybrid materials combining the properties of both moieties. Due to synergistic effects and despite the anisometry of the cluster compounds, individual properties such as liquid-crystalline phase stability of the organic part and emission abilities of its inorganic counter-part are enhanced in the hybrid compounds.

Introduction

The ability of crown ethers and azacrowns to selectively form coordination complexes with certain metal salts[1] established supramolecular chemistry as a new research topic with diverse applications such as molecular recognition, sensors, membranes, catalysis and more recently molecular motors pioneered by Sauvage, Stoddart and Feringa.[2] Many research studies address the development of liquid-crystalline crown ethers and azacrowns.[3] Grafting mesogenic groups together with flexible alkyl or perfluorinated side chains to the crown core resulted in nanosegregation of immiscible parts and thus liquid-crystalline self-assembly, which is further stabilized by van der Waals and π–π interactions, hydrogen bonding, and dipolar and/or fluorophobic interactions.[4] Despite the plethora of known crown ether complexes using both main-group and transition metals as well as lanthanide ions,[5,6] the generation of luminescent liquid-crystalline hybrid materials based on crown ether metal complexes still remains challenging. To find suitable alternatives to lanthanide-containing materials, we focused on hybrid materials derived from inorganic nanoclusters of the general formula $[M_6Q_8{}^iX_6{}^a]^n$ (Q = chalcogen/halogen, X = anionic or neutral ligand, M = Mo, Re, W, i = *inner*, a = *apical*). They contain an octahedron of metal atoms, can be readily synthesized using high-temperature methods and display strong red-NIR phosphorescence.[7–9] Their functionalization can be realized by (a) covalent bonding of organic ligands to the *apical* position of the octahedral complex, (b) ionic self-assembly employing organic counterions and (c) supramolecular grafting of organic ligands such as crown ethers or poly(ethylene oxide)[10] chains to form hybrid materials.[11] The attachment of an organic ligand sphere to the nanocluster not only improves its solubility and processability but also enables liquid-crystalline self-assembly to clustomesogens.[12–14] We recently reported the control of the mesophase type of the clustomesogen by proper choice of the crown ether ligand.[15,16] Azacrowns with peripheral 4-cyanobiphenyl units tethered with flexible alkyl spacers to the crown yielded nematic mesophases,[15] while complexes with dibenzo[18]crown-6 *o*-terphenyl ligands formed columnar phases.[16]

[a]*Institut für Organische Chemie, Universität Stuttgart, Pfaffenwaldring 55, D-70569 Stuttgart, Germany. E-mail: sabine.laschat@oc.uni-stuttgart.de*
[b]*University of Rennes, CNRS, ISCR – UMR 6226, ScanMAT – UMS 2001, F-35000 Rennes, France. E-mail: yann.molard@univ-rennes1.fr*

† Electronic supplementary information (ESI) available: Experimental data of triphenylene derivatives **Tri(*n*)** (p. S2), mesomorphic properties of triphenylene derivatives **Tri(*n*)** (p. S5), POM textures (Fig. S2), DSC traces (Fig. S3–S18), XRD diffractograms (Fig. S19–S31), luminescence spectra (Fig. S32–S35), emission lifetime graphs (Fig. S36–S39), NMR spectra (Fig. S40–S42, pp. S24–S51). See DOI: 10.1039/c8dt03254h

Moreover, the mesogenic ligand affected the luminescence intensity by encapsulating the cluster anions in an organic matrix, which was utilized for the production of an efficient oxygen sensor.[16] As we anticipated better "isolation" in such clustomesogens by sterically more demanding ligands, we synthesized a series of tribenzo[18]crown-6 *o*-terphenyls **Ter(*n*)** and their corresponding triphenylenes **Tri(*n*)**, which were complexed with two inorganic nanoclusters $Cs_2[Mo_6Br_{14}]$ and $Cs_2[Mo_6I_8(C_2F_5COO)_6]$, respectively (Fig. 1). Analogous to the dibenzo[18]crown-6 *o*-terphenyl ligands,[16] we propose hybrid materials where the Cs^+ cations are complexed by the crown ether derivatives resulting in the formation of mesophases as shown in Fig. 1.

Experimental

NMR spectra were recorded on *Bruker Avance 300*, *Avance 400*, *Avance 500* and *Avance 700* spectrometers at room temperature with TMS as an internal standard. The multiplicities are abbreviated as follows: s (singlet), d (doublet), t (triplet), q (quartet), p (quintet), and m (multiplet). 2D NMR spectra (COSY, HSQC, and HMBC) were measured to assign the signals. FT-IR spectra were recorded on a *Bruker ALPHA* device with a *Platinum ATR* system at room temperature. The intensities are abbreviated as follows: w (weak), m (medium), s (strong), and vs (very strong). MALDI-TOF mass spectra were recorded on a *Bruker Reflex IV* spectrometer. ESI mass spectra were recorded on a *Bruker Daltonics mikrO-TOF-Q* spectrometer. For polarizing optical microscopy (POM), an *Olympus BX50* microscope with a *Linkam TP93* control unit was used. Differential scanning calorimetry (DSC) was performed on a *Mettler Toledo DSC 822e* device. DSC samples were prepared in aluminum pans (40 μL) from *Mettler Toledo*. X-ray diffraction measurements (SAXS and WAXS) were conducted on a *Bruker Nanostar C* device with a *HI-STAR* detector using $Cu_{K\alpha}$ radiation (λ = 1.54056 Å). For thin layer chromatography (TLC), aluminum plates (precoated with silica gel 60 F_{254}) from *Merck* were used. Column chromatography was performed with silica gel (grain size 40–63 μm) from *Fluka*. If not mentioned otherwise, all commercial chemicals were used as received. Dry solvents were distilled under a nitrogen atmosphere using common drying agents prior to use. Moisture and/or oxygen sensitive reactions were conducted using common Schlenk techniques. ^{133}Cs solid-state NMR experiments were performed on a *Bruker 600 Avance III* spectrometer. The magic angle spinning frequency was set to 15 kHz with a 3.2 mm MAS probe head. A solid echo pulse sequence was used with a pulse length set to 1.31 μs and an echo delay set to 1.33 μs corresponding to 20 rotor periods. The recycle delay was set to 2 s. ^{133}Cs NMR spectra were referenced to a 0.2 M CsBr solution (δ_{iso} = 0 ppm). Lifetime measurements and TRPL mapping were realized using a pico-

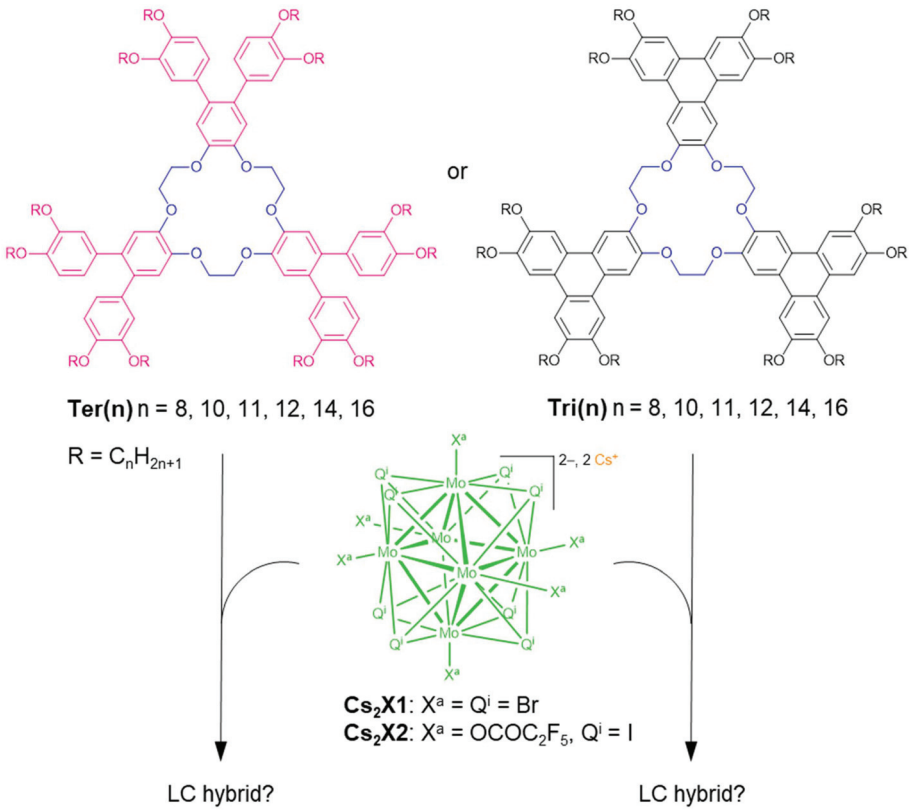

Fig. 1 Structures of the *o*-terphenyl and triphenylene crown ethers **Ter(*n*)** and **Tri(*n*)**, respectively, and the metal cluster compounds Cs_2X used in this study for the possible formation of liquid-crystalline hybrids.

second laser diode (*Jobin Yvon deltadiode*, 375 nm) and a *Hamamatsu C10910-25* streak camera mounted with a slow single sweep unit. Signals were integrated on a 30 nm bandwidth. Fits were obtained using the *Origin* software and the goodness of fit was judged from the reduced χ^2 value and the residual plot shape. The absolute quantum yields (AQYs) were measured with a *C9920-03 Hamamatsu* system equipped with a 150 W xenon lamp, a monochromator, an integrating sphere and a red-NIR sensitive *PMA-12* detector.

Synthesis

Borolanes **3(*n*)** were prepared according to ref. 17.

Clusters **Cs_2X1** and **Cs_2X2** were synthesized according to reported procedures.[18,19]

Hexabromotribenzo[18]crown-6 (2)

Bromine (94 μL, 293 mg, 3.68 mmol, in 1.5 mL CH_2Cl_2) was added to a solution of tribenzo[18]crown-6 **1** (200 mg, 491 μmol) in CH_2Cl_2 (3.0 mL) and the resulting mixture was stirred for 45 min at room temperature and subsequently refluxed for 5 h. After cooling to room temperature, NaOH (1 M, 10 mL) and sat. Na_2SO_3 solution (10 mL) were added and the phases were separated. The aqueous phase was extracted with CH_2Cl_2 (3 × 20 mL), the combined organic layers were washed with water (2 × 15 mL) and dried ($MgSO_4$) and the solvent was removed under reduced pressure. The resulting crude solid was purified by recrystallization from acetone to yield the product **2** as a colorless solid (277 mg, 311 μmol, 63%). ^{1}H NMR (300 MHz, $CDCl_3$): δ = 4.32 (s, 12H, a-H), 7.11 (s, 6H, 3-H, 6-H) ppm. ^{13}C NMR (75 MHz, $CDCl_3$): δ = 67.5 (C-a), 115.7 (C-4, C-5), 119.1 (C-3, C-6), 148.3 (C-1, C-2) ppm. FT-IR (ATR): $\tilde{\nu}$ = 3109 (w), 2928 (w), 2877 (w), 1720 (w), 1585 (w), 1492 (vs), 1451 (s), 1403 (w), 1378 (w), 1353 (s), 1326 (m), 1241 (s), 1198 (vs), 1119 (m), 1056 (m), 946 (m), 872 (m), 851 (m), 801 (m), 709 (w), 650 (m) cm^{-1}. HRMS (ESI): *m*/*z* calcd for $[C_{24}H_{18}Br_6O_6Na]^+$: 904.6037, found: 904.6036.

General procedure for the synthesis of *o*-terphenyl crown ethers Ter(*n*) by Suzuki coupling (GP 1)

Following a procedure from Wöhrle,[4e] hexabromotribenzo[18]crown-6 **2** (100 mg, 113 μmol, 1 eq.), Na_2CO_3 (1.44 g, 13.6 mmol, 120 eq.), $Pd(PPh_3)_4$ (26.1 mg, 22.6 μmol, 0.2 eq.) and degassed water (15 mL) were mixed under an atmosphere of N_2. The respective borolane **3(*n*)** (1.02 mmol, 9 eq.) was dissolved in degassed dimethoxyethane (DME, 15 mL) and subsequently added at room temperature. The resulting mixture was refluxed for 16 h. The inert atmosphere was removed and the mixture was stirred for further 5 h at 130 °C. After cooling, the mixture was extracted with CH_2Cl_2 (3 × 20 mL), the combined organic layers were washed with water (3 × 15 mL) and dried ($MgSO_4$), and the solvent was removed under reduced pressure. The resulting black oil was dissolved in petroleum ether (20 mL), then ethylenediamine (4 mL) was added and the mixture was stirred for 16 h at room temperature. The colorless solution was filtered through a silica pad, eluted with CH_2Cl_2 (200 mL) and the resulting organic phase was washed with water (100 mL) and dried ($MgSO_4$) and the solvent was removed under reduced pressure. The crude product was recrystallized from acetone/2-propanol and subsequently chromatographed on silica to yield the desired product **Ter(*n*)** as a colorless solid.

4,4′,4″,5,5′,5″-Hexakis[3‴,4‴-bis(octyloxy)phenyl]tribenzo[18]crown-6 [Ter(8)]. Synthesis was carried out according to GP 1 with borolane **3(8)** (470 mg, 1.02 mmol). Purification was done by recrystallization (acetone/2-propanol, 7/13, v/v) and subsequent column chromatography (SiO_2, hexanes : ethyl acetate = 15 : 1 → 5 : 1, R_f = 0.2). Yield: 71% (189 mg, 78.6 μmol), colorless solid. ^{1}H NMR (500 MHz, $CDCl_3$): δ = 0.84–0.92 (m, 36H, CH_3), 1.22–1.39 (m, 120H, CH_2), 1.59–1.67 (m, 12H, OCH_2CH_2), 1.75–1.84 (m, 12H, OCH_2CH_2), 3.66 (t, *J* = 6.7 Hz, 12H, OCH_2), 3.93 (t, *J* = 6.7 Hz, 12H, OCH_2), 4.50 (s, 12H, a-H), 6.56 (d, *J* = 2.0 Hz, 6H, 2′-H), 6.68 (dd, *J* = 8.3 Hz, 2.0 Hz, 6H, 6′-H), 6.73 (d, *J* = 8.3 Hz, 6H, 5′–H), 6.99 (s, 6H, 3-H) ppm. ^{13}C NMR (126 MHz, $CDCl_3$): δ = 14.1 (CH_3), 22.7, 22.7, 26.0, 26.1, 29.1, 29.3, 29.4, 29.4, 29.5, 31.9, 31.9 (CH_2), 68.1 (C-a), 69.1, 69.3 (OCH_2), 113.3 (C-5′), 116.1 (C-2′), 117.2 (C-3), 121.8 (C-6′), 133.8, 134.2 (C-4, C-1′), 147.7, 147.8, 148.4 (C-1, C-2, C-3′, C-4′) ppm. FT-IR (ATR): $\tilde{\nu}$ = 2954 (m), 2922 (s), 2854 (m), 1603 (w), 1577 (w), 1557 (w), 1494 (s), 1468 (m), 1433 (w), 1415 (w), 1378 (w), 1247 (vs), 1195 (m), 1166 (w), 1137 (m), 1064 (m), 1025 (m), 970 (w), 859 (w), 807 (w), 723 (w), 616 (w), 470 (w) cm^{-1}. MS (MALDI-TOF): *m*/*z* calcd for $[C_{156}H_{240}O_{18}{}^+$ $(M^+)]$: 2402.8; found: 2397.2. CHN analysis calcd (%) for $C_{156}H_{240}O_{18}$ (2403.62): C 77.95, H 10.06; found: C 77.72, H 9.85.

4,4′,4″,5,5′,5″-Hexakis[3‴,4‴-bis(decyloxy)phenyl]tribenzo[18]crown-6 [Ter(10)]. Synthesis was carried out according to GP 1 with borolane **3(10)** (527 mg, 1.02 mmol). Purification was done by recrystallization (acetone/2-propanol, 5/15, v/v) and subsequent column chromatography (SiO_2, hexanes : ethyl acetate = 20 : 1 → 10 : 1, R_f = 0.3). Yield: 69% (209 mg, 78.6 μmol), colorless solid. ^{1}H NMR (500 MHz, $CDCl_3$): δ = 0.84–0.92 (m, 36H, CH_3), 1.20–1.50 (m, 168H, CH_2), 1.59–1.67 (m, 12H, OCH_2CH_2), 1.75–1.83 (m, 12H, OCH_2CH_2), 3.66 (t, *J* = 6.7 Hz, 12H, OCH_2), 3.93 (t, *J* = 6.7 Hz, 12H, OCH_2), 4.50 (s, 12H, a-H), 6.55 (d, *J* = 1.9 Hz, 6H, 2′-H), 6.68 (dd, *J* = 8.3 Hz, 1.9 Hz, 6H, 6′-H), 6.73 (d, *J* = 8.3 Hz, 6H, 5′–H), 6.99 (s, 6H, 3-H) ppm. ^{13}C NMR (126 MHz, $CDCl_3$): δ = 14.1 (CH_3), 22.7, 26.1, 26.1, 29.2, 29.4, 29.4, 29.4, 29.5, 29.5, 29.6, 29.6, 29.7, 29.7, 29.7, 31.9, 32.0 (CH_2), 68.1 (C-a), 69.1, 69.3 (OCH_2), 113.3 (C-5′), 116.1 (C-2′), 117.2 (C-3), 121.8 (C-6′), 133.8, 134.2 (C-4, C-1′), 147.7, 148.4 (C-1, C-2, C-3′, C-4′) ppm. FT-IR (ATR): $\tilde{\nu}$ = 2920 (s), 2852 (s), 1603 (w), 1577 (w), 1557 (w), 1494 (s), 1468 (m), 1378 (w), 1247 (vs), 1194 (m), 1167 (m), 1137 (m), 1064 (m), 941 (w), 859 (w), 806 (w), 722 (w), 616 (w), 467 (w) cm^{-1}. MS (MALDI-TOF): *m*/*z* calcd for $[C_{180}H_{288}O_{18}{}^+$ $(M^+)]$: 2739.2; found: 2735.2. CHN analysis calcd (%) for $C_{180}H_{288}O_{18}$ (2740.27): C 78.90, H 10.59; found: C 78.81, H 10.35.

4,4′,4″,5,5′,5″-Hexakis[3‴,4‴-bis(undecyloxy)phenyl]tribenzo[18]crown-6 [Ter(11)]. Synthesis was carried out according to GP 1 with borolane **3(11)** (556 mg, 1.02 mmol). Purification was done by recrystallization (acetone/2-propanol, 10/5, v/v).

Yield: 34% (113 mg, 38.9 μmol), colorless solid. ^{1}H NMR (500 MHz $CDCl_3$): δ = 0.79–0.82 (m, 36H, CH_3), 1.15–1.40 (m, 168H, CH_2), 1.53–1.59 (m, 12H, OCH_2CH_2), 1.69–1.75 (m, 12H, OCH_2CH_2), 3.57–3.60 (m, 12H, OCH_2), 3.84–3.87 (m, 12H, OCH_2), 4.43 (s, 12H, a-H), 6.48 (d, J = 1.3 Hz, 6H, 2′-H), 6.61 (dd, J = 8.2 Hz, 1.3 Hz, 6H, 2′-H), 6.66 (d, J = 8.2 Hz, 6H, 5′-H), 6.92 (s, 12H, 3-H) ppm. ^{13}C NMR (125 MHz, $CDCl_3$): δ = 14.2 (CH_3), 22.7, 26.1, 26.1, 29.2, 29.4, 29.4, 29.5, 29.6, 29.7, 29.7, 29.8, 32.0, 32.0 (CH_2), 68.1 (C-a), 69.1, 69.3 (OCH_2), 116.0 (C-5′), 117.2 (C-2′), 121.8 (C-6′), 133.8, 134.2 (C-4, C-1′), 147.7, 148.3 (C-1, C-2, C-3′, C-4′) ppm. FT-IR (ATR): $\tilde{\nu}$ = 2920 (vs), 2852 (s), 1603 (w), 1557 (w), 1494 (s), 1468 (m), 1378 (w), 1247 (vs), 1194 (s), 1136 (m), 1064 (m), 951 (w), 859 (w), 806 (w), 721 (w) cm^{-1}. MS (MALDI-TOF): m/z calcd for [$C_{192}H_{312}O_{18}^+$ (M^+)]: 2908.3; found: 2905.0. CHN analysis calcd (%) for $C_{192}H_{312}O_{18}$ (2908.59): C 79.29, H 10.81; found: C 79.33, H 10.63.

4,4′,4″,5,5′,5″-Hexakis[3‴,4‴-bis(dodecyloxy)phenyl]tribenzo[18]crown-6 [Ter(12)]. Synthesis was carried out according to GP 1 with borolane **3(12)** (585 mg, 1.02 mmol). Purification was done by recrystallization (acetone/2-propanol, 10/5, v/v). Yield: 68% (237 mg, 77.0 μmol), colorless solid. ^{1}H NMR (500 MHz $CDCl_3$): δ = 0.87–0.89 (m, 36H, CH_3), 1.22–1.41 (m, 192H, CH_2), 1.60–1.66 (m, 12H, OCH_2CH_2), 1.75–1.81 (m, 12H, OCH_2CH_2), 3.64–3.67 (m, 12H, OCH_2), 3.91–3.94 (m, 12H, OCH_2), 4.50 (s, 12H, a-H), 6.54 (d, J = 1.9 Hz, 6H, 2′-H), 6.68 (dd, J = 8.3 Hz, 1.9 Hz, 6H, 2′-H), 6.73 (d, J = 8.3 Hz, 6H, 5′-H), 6.99 (s, 12H, 3-H) ppm. ^{13}C NMR (125 MHz, $CDCl_3$): δ = 14.1 (CH_3), 22.7, 26.1, 26.1, 29.2, 29.4, 29.4, 29.5, 29.6, 29.7, 29.7, 29.8, 29.8, 29.8, 32.0 (CH_2), 68.1 (C-a), 69.1, 69.3 (OCH_2), 116.1 (C-5′), 117.3 (C-2′), 121.8 (C-6′), 133.8, 134.2 (C-4, C-1′), 147.7, 148.4 (C-1, C-2, C-3′, C-4′) ppm. FT-IR (ATR): $\tilde{\nu}$ = 2920 (vs), 2852 (s), 1603 (w), 1577 (w), 1557 (w), 1494 (s), 1468 (m), 1378 (w), 1311 (w), 1247 (vs), 1195 (s), 1137 (m), 1065 (m), 1030 (w), 965 (w), 894 (w), 859 (w), 806 (w), 721 (w) 630 (s), 537 (m) cm^{-1}. MS (MALDI-TOF): m/z calcd for [$C_{204}H_{336}O_{18}^+$ (M^+)]: 3076.5; found: 3073.4. CHN analysis calcd (%) for $C_{204}H_{336}O_{18}$ (3076.91): C 79.63, H 11.01; found: C 79.57, H 10.70.

4,4′,4″,5,5′,5″-Hexakis[3‴,4‴-bis(tetradecyloxy)phenyl]tribenzo[18]crown-6 [Ter(14)]. Synthesis was carried out according to GP 1 with borolane **3(14)** (640 mg, 1.02 mmol). Purification was done by recrystallization (acetone/2-propanol, 5/15, v/v) and subsequent column chromatography (SiO_2, hexanes : ethyl acetate = 25 : 1 → 10 : 1, R_f = 0.6). Yield: 72% (278 mg, 81.4 μmol), colorless solid. ^{1}H NMR (500 MHz, $CDCl_3$): δ = 0.88 (t, J = 6.7 Hz, 36H, CH_3), 1.20–1.49 (m, 264H, CH_2), 1.59–1.67 (m, 12H, OCH_2CH_2), 1.75–1.83 (m, 12H, OCH_2CH_2), 3.65 (t, J = 6.7 Hz, 12H, OCH_2), 3.93 (t, J = 6.7 Hz, 12H, OCH_2), 4.50 (s, 12H, a-H), 6.55 (d, J = 1.9 Hz, 6H, 2′-H), 6.68 (dd, J = 8.3 Hz, 1.9 Hz, 6H, 6′-H), 6.73 (d, J = 8.3 Hz, 6H, 5′-H), 6.99 (s, 6H, 3-H) ppm. ^{13}C NMR (126 MHz, $CDCl_3$): δ = 14.1 (CH_3), 22.7, 26.1, 26.1, 29.2, 29.4, 29.4, 29.5, 29.5, 29.7, 29.7, 29.8, 29.8, 29.8, 32.0 (CH_2), 68.1 (C-a), 69.1, 69.3 (OCH_2), 113.3 (C-5′), 116.1 (C-2′), 117.3 (C-3), 121.8 (C-6′), 133.8, 134.2 (C-4, C-1′), 147.8, 148.4 (C-1, C-2, C-3′, C-4′) ppm. FT-IR (ATR): $\tilde{\nu}$ = 2919 (vs), 2851 (s), 1727 (w), 1603 (w), 1577 (w), 1558 (w), 1495 (s), 1467 (s), 1378 (w), 1248 (vs), 1195 (m), 1166 (w), 1137 (m), 1064 (m), 1023 (m), 943 (w), 859 (w), 805 (w), 721 (w), 616 (w), 468 (w) cm^{-1}. MS (MALDI-TOF): m/z calcd for [$C_{228}H_{384}O_{18}^+$ (M^+)]: 3412.9; found: 3408.3. CHN analysis calcd (%) for $C_{228}H_{384}O_{18}$ (3413.56): C 80.22, H 11.34; found: C 80.51, H 11.07.

4,4′,4″,5,5′,5″-Hexakis[3‴,4‴-bis(hexadecyloxy)phenyl]tribenzo[18]crown-6 [Ter(16)]. Synthesis was carried out according to GP 1 with borolane **3(16)** (527 mg, 1.02 mmol). Purification was done by recrystallization (acetone/2-propanol, 5/15, v/v) and subsequent column chromatography (SiO_2, hexanes : ethyl acetate = 20 : 1 → 10 : 1, R_f = 0.8). Yield: 72% (346 mg, 78.6 μmol), colorless solid. ^{1}H NMR (700 MHz, $CDCl_3$): δ = 0.84–0.90 (m, 36H, CH_3), 1.19–1.48 (m, 312H, CH_2), 1.63 (p, J = 6.8 Hz, 12H, OCH_2CH_2), 1.78 (p, J = 6.8 Hz, 12H, OCH_2CH_2), 3.65 (t, J = 6.7 Hz, 12H, OCH_2), 3.93 (t, J = 6.7 Hz, 12H, OCH_2), 4.50 (s, 12H, a-H), 6.55 (d, J = 2.0 Hz, 6H, 2′-H), 6.68 (dd, J = 8.3 Hz, 2.0 Hz, 6H, 6′-H), 6.73 (d, J = 8.3 Hz, 6H, 5′-H), 6.99 (s, 6H, 3-H) ppm. ^{13}C NMR (176 MHz, $CDCl_3$): δ = 14.1 (CH_3), 22.7, 26.1, 26.1, 29.2, 29.4, 29.4, 29.4, 29.5, 29.5, 29.6, 29.7, 29.7, 29.7, 29.8, 29.8, 29.8, 29.8, 32.0 (CH_2), 68.2 (C-a), 69.1, 69.3 (OCH_2), 113.4 (C-5′), 116.1 (C-2′), 117.3 (C-3), 121.8 (C-6′), 133.8, 134.2 (C-4, C-1′), 147.8, 148.4 (C-1, C-2, C-3′, C-4′) ppm. FT-IR (ATR): $\tilde{\nu}$ = 2916 (vs), 2849 (s), 1603 (w), 1557 (w), 1494 (m), 1467 (m), 1379 (w), 1247 (s), 1194 (m), 1166 (w), 1136 (m), 1066 (m), 1017 (w), 955 (w), 908 (w), 860 (w), 807 (w), 722 (m), 648 (w), 616 (w), 465 (w) cm^{-1}. MS (MALDI-TOF): m/z calcd for [$C_{252}H_{432}O_{18}^+$ (M^+)]: 3749.3; found: 3744.0. HRMS (ESI): m/z calcd for [$C_{252}H_{432}O_{18}Na$]$^+$: 3772.2849, found: 3772.2849. CHN analysis calcd (%) for $C_{252}H_{432}O_{18}$ (3750.21): C 80.71, H 11.61; found: C 80.62, H 11.66.

The respective experimental data of the triphenylene derivatives **Tri(*n*)** are listed in the ESI† (pp. S2–S5).

General procedure for the synthesis of *o*-terphenyl-tribenzo[18]crown-6 hybrids Ter(*n*)·$Cs_{0.5}X_{0.25}$ (GP 2)

Following a procedure from Pedersen,[20] the respective *o*-terphenyl crown ether **Ter(14)** or **Ter(16)** (17.6 μmol, 1 eq.) was dissolved in CH_2Cl_2 (5 mL). The respective molybdato cluster $\mathbf{Cs_2X}$ (4.57 μmol, 0.26 eq.) was dissolved in acetonitrile (5 mL) and added to the solution. The resulting mixture was stirred for 16 h at room temperature. The solvents were removed under reduced pressure, the residue was taken up in CH_2Cl_2 (10 mL), filtered and the solvent was removed under reduced pressure to yield the complexes **Ter(14)·$Cs_{0.5}X_{0.25}$** and **Ter(16)·$Cs_{0.5}X_{0.25}$** as yellow to orange solids (17.58 μmol) in quantitative yields.

Results and discussion

Synthesis of the tribenzo[18]crown-6 derivatives and clustomesogens

The synthesis of the *o*-terphenyls **Ter(*n*)** and triphenylenes **Tri(*n*)** (n = 8, 10, 11, 12, 14, 16) as well as the synthesis of the crown ether complexes **Ter(14)·$Cs_{0.5}X_{0.25}$** and **Ter(16)·$Cs_{0.5}X_{0.25}$** are depicted in Scheme 1. Six-fold bromination of the known

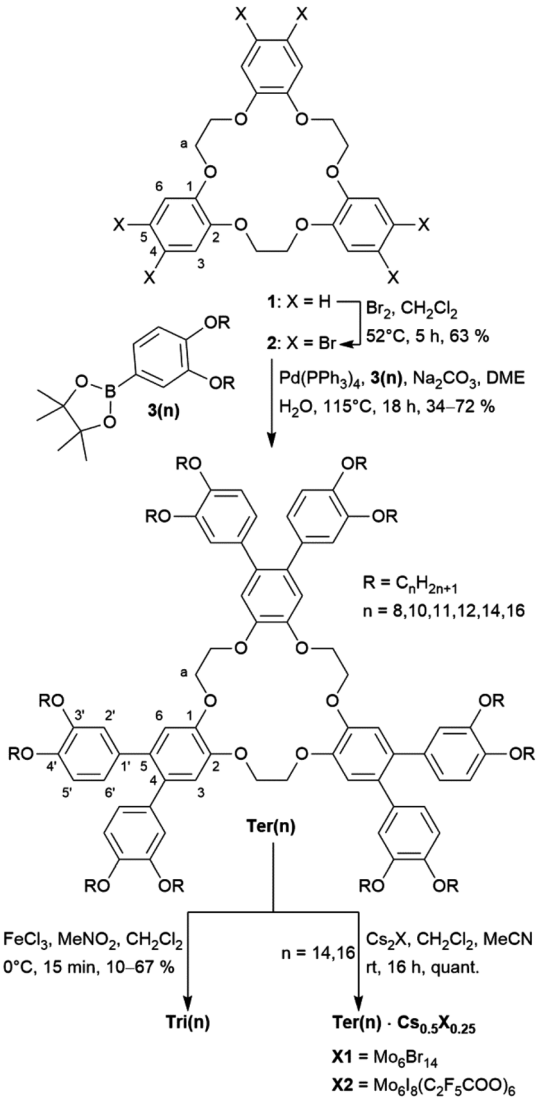

Scheme 1 Synthesis of the *o*-terphenyl **Ter(*n*)**, triphenylene **Tri(*n*)** and *o*-terphenyl cluster **Ter(14)·Cs$_{0.5}$X$_{0.25}$** and **Ter(16)·Cs$_{0.5}$X$_{0.25}$** derivatives.

tribenzo[18]crown-6 **1**[21] provided hexabromotribenzo[18]crown-6 **2** in 63% yield, which was converted to the *o*-terphenyl crown ether **Ter(*n*)** by six-fold Suzuki cross-coupling with the respective pinacol borolane **3(*n*)**. The crude product **Ter(*n*)** required treatment with ethylenediamine in order to remove the residual Pd catalyst that had been complexed with the crown. After purification by column chromatography, the product **Ter(*n*)** was isolated in 34–72% yield. A subsequent Scholl reaction with $FeCl_3$ in $MeNO_2/CH_2Cl_2$ at 0 °C yielded triphenylene **Tri(*n*)** in 10–67%. Presumably, the low yield of **Tri(16)** was caused by the poor solubility of the precursor **Ter(16)** in cold CH_2Cl_2. Longer reaction times and changing the oxidation system to $DDQ/MeSO_3H/CH_2Cl_2$ or $MoCl_5/CH_2Cl_2$ resulted in either the decomposition of the triphenylene products or lower yields.

According to former studies by Pedersen and Nakamura, the cavity of [18]crown-6 derivatives is too small to accommodate the cesium cation and thus a 2 : 1 stoichiometry of ligand/Cs^+ was found.[22] This proposed model is also in good agreement with recent results by Chu, who utilized crown ether-modified copolymers to obtain experimental evidence for the strong tendency of Cs^+ to form sandwich-type crown ether/metal complexes.[23] Therefore, the complexed derivatives **Ter(14)·Cs$_{0.5}$X$_{0.25}$** and **Ter(16)·Cs$_{0.5}$X$_{0.25}$** were synthesized from the cluster salts **Cs$_2$X1** and **Cs$_2$X2** (**X1** = $[Mo_6Br_{14}]^{2-}$; **X2** = $[Mo_6I_8(C_2F_5COO)_6]^{2-}$) in a ratio of 2 : 1 (ligand/Cs^+) following a procedure by Pedersen,[20] using a mixture of CH_2Cl_2 and acetonitrile to achieve good solubility of both the cluster salt and the respective crown ether. The desired clustomesogens were obtained in quantitative yields.

We surmised that clustomesogens with short chain lengths (n = 8, 10, 12) might lead to high clearing transitions close to the decomposition temperature and thus complex formation was limited to the crown ethers with C_{14} and C_{16} chains.

Interactions between the Cs^+ cations of the ternary salts and **Ter(14)** are very well illustrated by magic angle spinning (MAS) solid-state ^{133}Cs NMR experiments. However, the spectra of crystalline **Cs$_2$X1** and **Cs$_2$X2** contain two sharp signals at 36.7 ppm and 216 ppm, and at −4.97 ppm and −107 ppm, respectively, only one broad signal at −18 ppm appears for hybrids **Ter(14)·Cs$_{0.5}$X$_{0.25}$** (see ESI Fig. S40† for spectra). The fact that only one signal is observed for the hybrid compounds demonstrates the equivalence of the two Cs^+ cations. As the signals of the two hybrids have the same chemical shift, this shows that the cations interact poorly with the cluster inner and apical ligands. This last point is in good accordance with the bulkiness of the central core of **Ter(*n*)** ligands.

Surprisingly, upon attempted complexation of the corresponding triphenylenes **Tri(14)** and **Tri(16)** with cluster salts under analogous conditions, the decomposition of the crown ethers was observed. Presumably, the tribenzo[18]crown-6 triphenylenes **Tri(*n*)** are too rigid to accommodate the bulky cluster anion or the cluster anion promotes ether cleavage. The experimental observation is in good agreement with previous work by Reiner,[24] who studied the oxidative lignine cleavage catalyzed by polyoxometallate anions. Furthermore, Marks,[25] Quaranta,[26] Keith[27] and Anwander[28] have also reported ether cleavage induced by lanthanide triflates and other high-valent metal salts.

Mesomorphic properties of the *o*-terphenyl tribenzo[18]crown-6 derivatives

All *o*-terphenyl compounds **Ter(*n*)** showed mesomorphic properties under a polarizing microscope (POM) and exhibited fan-shaped textures typical of columnar mesophases. Illustrative examples are shown for **Ter(8)** (Fig. 2a) and **Ter(12)** (Fig. 2b). In the case of **Ter(16)**, upon cooling from the isotropic phase, uncharacteristic textures appeared at 85 °C, whose color changed upon cooling below 56 °C, suggesting the presence of a second mesophase (see ESI Fig. S2†). Differential scanning calorimetry (DSC) measurements revealed enantiotropic behavior for all *o*-terphenyls **Ter(*n*)** (Table 1). For **Ter(8)**,

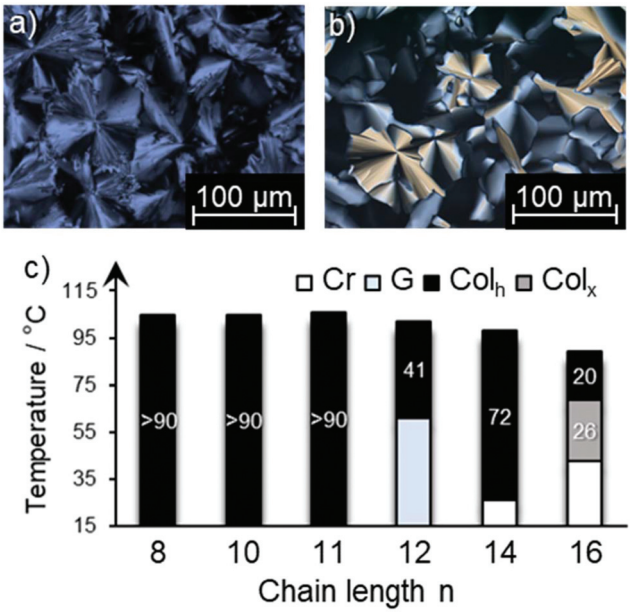

Fig. 2 (a) Fan-shaped POM textures of **Ter(8)** (103 °C, 5 K min^{-1}) and (b) **Ter(12)** (95 °C, 10 K min^{-1}) upon cooling from the isotropic phase (magnification: ×200). (c) Temperature ranges in K of the mesophases of *o*-terphenyls **Ter(*n*)** for different chain lengths *n*. The phase transitions and phase widths were determined by DSC upon 2nd cooling. The DSC curves are shown in Fig. S3–S8 in the ESI.†

Ter(10) and **Ter(11)** with shorter chain lengths, neither melting transition nor crystallization could be observed in the DSC thermograms (see ESI Fig. S3–S5†). Thus, the mesophase was stable from sub-ambient temperatures to 105 °C. For the higher homologues, melting points were observed at 26 °C for **Ter(14)** and then increased to 43 °C for **Ter(16)**, while clearing transitions steadily decreased from 98 °C for **Ter(14)** to 89 °C for **Ter(16)**, resulting in relatively broad phase widths (Fig. 2c). In the case of **Ter(16)**, a second columnar mesophase was detected between 69 °C and 43 °C in the DSC curves.

In order to assign the phase geometries, X-ray diffraction (XRD) measurements were performed (Table 2). All *o*-terphenyls **Ter(*n*)** displayed a diffuse halo in the wide-angle region (WAXS) between 4.2 Å and 4.5 Å, which is caused by the molten alkoxy chains in the mesophase. The small-angle (SAXS) profiles of compounds **Ter(8)** and **Ter(10)** showed three distinct reflexes in a ratio of $1:1/\sqrt{3}:1/2$, which could be indexed to (10), (11), and (20), which are characteristic of Col$_h$ phases with the *p6mm* symmetry (Fig. 3). The other *o*-terphenyl compounds **Ter(*n*)** (*n* = 12, 14, 16) only showed the (10) and (11) reflexes. Despite the absence of higher order reflections, a Col$_h$ phase was assumed due to their structural similarity to **Ter(8)** and **Ter(10)**. The lattice parameters *a* increased with increasing chain lengths from 35.10 Å for **Ter(8)** to 45.61 Å for **Ter(16)** (Table 2). The lower-temperature mesophase (Col$_x$) of compound **Ter(16)** displayed similar small-angle reflections compared to the corresponding Col$_h$ phase at higher temperatures. However, a wide-angle halo appeared at 4.2 Å and an increased lattice parameter *a* = 46.82 Å was found, suggesting that the alkoxy side chains were more tightly packed in an expanded hexagonal lattice of the low temperature phase, whereas lattice shrinkage in the high temperature phase resulted in a larger volume requirement of the alkoxy chains.

The mesomorphic properties of the respective triphenylene derivatives **Tri(*n*)** are discussed in the ESI† (pp. S5–S7).

Mesomorphic properties of the *o*-terphenyl tribenzo[18]crown-6 clusters

All the clustomesogens **Ter(*n*)·Cs$_{0.5}$X$_{0.25}$** show typical textures for Col$_h$ mesophases under the POM upon cooling from the isotropic phase, as illustrated in Fig. 4 for **Ter(14)·Cs$_{0.5}$X2$_{0.25}$** and **Ter(16)·Cs$_{0.5}$X1$_{0.25}$**. Under UV irradiation (see Fig. 4b and d), these compounds emitted red light, verifying the hybrid character of these species and the homogeneity of the samples.

DSC traces of the hybrids show enantiotropic mesomorphism for **Ter(*n*)·Cs$_{0.5}$X1$_{0.25}$**. The clearing temperatures of these compounds (147 °C and 125 °C, see Fig. 5) increased drastically compared to those of the neat crown ethers **Ter(14)** and **Ter(16)**, whereas crystallization points remain unchanged, leading to significantly broadened mesophases of 123 K and 104 K, respectively. The clustomesogens **Ter(*n*)·Cs$_{0.5}$X2$_{0.25}$** exhibited slightly higher clearing temperatures (159 °C

Table 1 DSC results of the different crown ether derivatives (2nd cooling). Phase transition temperatures *T* are given in °C and the transition enthalpies in kJ mol^{-1}.[a,b] **X1** = $[Mo_6Br_{14}]^{2-}$, **X2** = $[Mo_6I_8(C_2F_5COO)_6]^{2-}$

Compound	Cr	T_m (ΔH)	Col$_x$	T (ΔH)	Col$_h$	T_c (ΔH)	I
Ter(8)	—	—	—	—	●	105 (−10.0)	●
Ter(10)	—	—	—	—	●	105 (−9.9)	●
Ter(11)	—	—	—	—	●	105 (−10.8)	●
Ter(12)	G	61 (—)	—	—	●	102 (−9.9)	●
Ter(14)	●	26 (−65.0)	—	—	●	98 (−16.1)	●
Ter(16)	●	43 (−127)	●	69 (−12.9)	●	89 (−7.1)	●
Ter(14)·Cs$_{0.5}$X1$_{0.25}$	●	24 (−51.8)	—	—	●	147 (−3.87)	●
Ter(16)·Cs$_{0.5}$X1$_{0.25}$	●	42 (−117)	—	—	●	125 (−0.45)	●
Ter(14)·Cs$_{0.5}$X2$_{0.25}$	—	—	—	—	●	159 (−8.57)	●
Ter(16)·Cs$_{0.5}$X2$_{0.25}$ [c]	—	—	—	—	●	150 (−4.65)	●

[a] Heating/cooling rate: 5 K min^{-1}. [b] The following phases were observed: crystalline Cr, glass G, columnar hexagonal Col$_h$, columnar Col$_x$, isotropic I. [c] An additional crystal-to-crystal transition was detected at 36 °C upon 2nd heating.

Table 2 Results of the XRD experiments for the *o*-terphenyls **Ter(*n*)**

Ter(*n*)	Mesophase	Lattice spacing/Å	*d* spacing/Å exp. (calcd.)	Miller indices
Ter(8)	Col_h	a = 35.10	30.40	(10)
	p6mm (61 °C)		17.52 (17.55)	(11)
			15.29 (15.20)	(20)
			4.4	Halo
Ter(10)	Col_h	a = 39.36	34.09	(10)
	p6mm (70 °C)		19.62 (19.68)	(11)
			17.03 (17.04)	(20)
			4.5	Halo
Ter(12)	Col_h	a = 40.07	34.70	(10)
	p6mm (90 °C)		4.5	Halo
Ter(14)	Col_h	a = 45.06	39.02	(10)
	p6mm (45 °C)		4.4	Halo
Ter(16)	Col_h	a = 46.82	40.51	(10)
	p6mm (54 °C)		23.47 (23.39)	(11)
			4.2	Halo
	Col_h	a = 45.61	39.50	(10)
	p6mm (70 °C)		22.99 (22.80)	(11)
			4.5	Halo

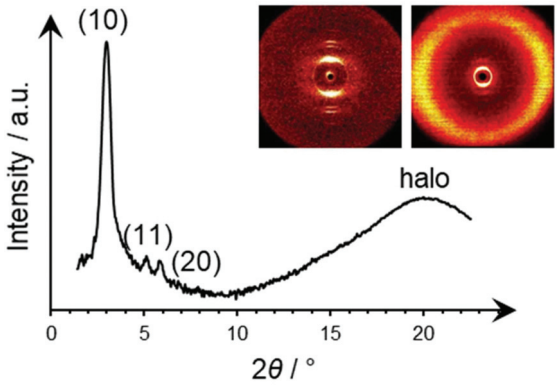

Fig. 3 WAXS diffractogram of an oriented **Ter(8)** fiber at 61 °C upon heating with the corresponding diffraction patterns (left: SAXS and right: WAXS).

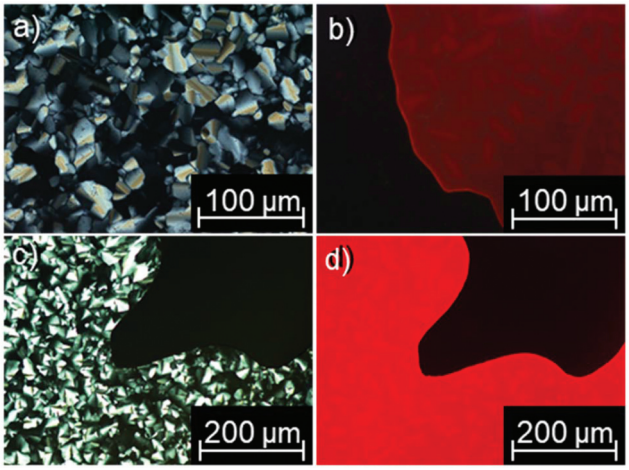

Fig. 4 Linear defects of (a) **Ter(16)·Cs$_{0.5}$X1$_{0.25}$** (140 °C, 5 K min^{-1}, magnification: ×200), (b) **Ter(16)·Cs$_{0.5}$X1$_{0.25}$** under UV irradiation at 100 °C, (c) spherulite-like textures of **Ter(14)·Cs$_{0.5}$X2$_{0.25}$** (110 °C, 5 K min^{-1}, magnification: ×100) and (d) **Ter(14)·Cs$_{0.5}$X2$_{0.25}$** under UV irradiation at 130 °C. **X1** = $[Mo_6Br_{14}]^{2-}$ and **X2** = $[Mo_6I_8(C_2F_5COO)_6]^{2-}$. All pictures were taken upon cooling from the isotropic phase.

and 150 °C) than their corresponding counterpart **Ter(*n*)·Cs$_{0.5}$X1$_{0.25}$**. In contrast to **Ter(*n*)·Cs$_{0.5}$X1$_{0.25}$**, hybrids **Ter(*n*)·Cs$_{0.5}$X2$_{0.25}$** did not show crystallization upon cooling from the isotropic state; however a melting transition could be observed at 39 °C upon heating for **Ter(16)·Cs$_{0.5}$X2$_{0.25}$**.

It is well known from crown ethers[3c] and other liquid-crystalline macrocycles[29] that external guests have a pronounced effect on the mesomorphic properties. Mixed results were obtained regarding the effect of Cs^+ on the mesomorphism of crown ethers. For example, Shinkai reported a change of the helical pitch of cholesteric crown ethers upon complexation with Cs^+.[30] Previous work by our group revealed that complexation with Cs^+ salts often suppresses mesophase formation.[31] More recently, we discovered for structurally related crown ether clustomesogens that both the type of cluster anion and the replacement of K^+ by Cs^+ affected the temperature range and the geometry of the Col_h phase.[13a] Although both, cation and cluster anion, do have an influence on the mesophase stability, the difference in the clearing temperature and the transition enthalpy of the hybrids cannot be explained by a modulation of interactions between the Cs^+ cations and the cluster cores as ^{133}Cs chemical shifts observed for **Ter(14)·Cs$_{0.5}$X1$_{0.25}$** and **Ter(14)·Cs$_{0.5}$X2$_{0.25}$** are identical. Therefore, the cluster nature itself seems to have a direct influence on the liquid crystal phase stability.

XRD experiments confirmed the assumed Col_h mesophases by exhibiting three distinct (10), (11) and (20) reflexes in the small-angle section in a ratio of $1:1/\sqrt{3}:1/2$, as well as a diffuse halo in the wide-angle region (Table 3). The lattice parameters a for **Ter(*n*)·Cs$_{0.5}$X1$_{0.25}$** are lower (38.9 Å and 42.2 Å) than the a values for compounds **Ter(*n*)·Cs$_{0.5}$X2$_{0.25}$**

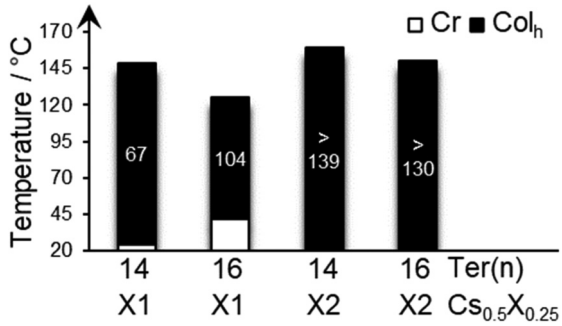

Fig. 5 Temperature ranges in K of the mesophases of hybrids **Ter(*n*)·$Cs_{0.5}X_{0.25}$** for different chain lengths *n*. **X1** = $[Mo_6Br_{14}]^{2-}$ and **X2** = $[Mo_6I_8(C_2F_5COO)_6]^{2-}$. The phase transitions and phase widths were determined by DSC upon 2nd/3rd cooling. The DSC curves are shown in Fig. S15–S18 in the ESI.†

(42.2 Å and 43.7 Å), which is possibly due to (i) a higher steric demand of the **X2** cluster anion in the intercolumnar area and (ii) differences in the electrostatic interaction strengths between cesium cations and **X1** or **X2** cluster anions. The diffuse halo appears for **Ter(*n*)·$Cs_{0.5}X1_{0.25}$** at 4.7 Å. For the hybrids **Ter(*n*)·$Cs_{0.5}X2_{0.25}$**, the halo could be observed at 4.3 Å, leading to a decreased π–π distance and more densely stacked columns. In comparison with the neat crown ethers **Ter(14)** and **Ter(16)** (45.0 Å, 45.6 Å, Table 2), the clustomesogens **Ter(*n*)·$Cs_{0.5}X_{0.25}$** surprisingly exhibit smaller lattice parameters ranging from 38.9 Å to 43.7 Å (Table 3). This might be explained by attractive ionic interactions between the double negatively charged cluster ions and the sandwiched cesium cations. From the obtained XRD data, we propose the packing model shown in Fig. 6. According to the model, each Cs^+ is sandwiched between two crown ether units and these sandwich complexes form the columns within the hexagonal lattice, while the cluster anions are embedded between the columns, so that the overall stoichiometry of the crown/Cs^+/cluster anion of 4 : 2 : 1 is maintained.

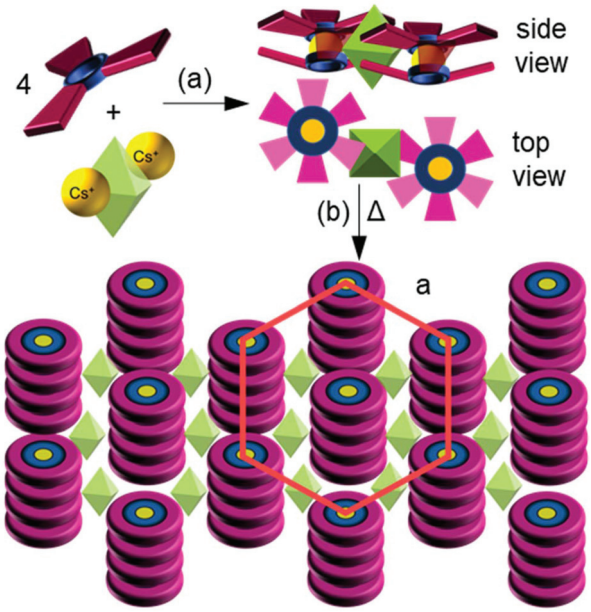

Fig. 6 Schematic overview of hybrid formation for crown ether ligands **Ter(14)** and **Ter(16)** with cluster salts **Cs_2X** in step (a) and self-assembly to the columnar hexagonal (Col$_h$) mesophase upon heating in step (b). The lower part of the figure shows the proposed packing model of the Col$_h$ phase based on the XRD data of the hybrids. The crown ether cesium sandwich complexes stacked along the columns are depicted as circles in the packing model for better clarity.

Luminescence properties of the *o*-terphenyl tribenzo[18]crown-6 clusters

As shown in Fig. 4b and d, the cluster compounds maintain their luminescence properties when complexed. As presented in Fig. 7, the emission spectra of **Ter(*n*)·$Cs_{0.5}X1_{0.25}$** at ambient temperature exhibited a broad emission band ranging from 550 nm to 950 nm (I_{max} at 708 nm) similar to that of **Cs_2X1**, whereas the emission spectra of the corresponding analogues **Ter(*n*)·$Cs_{0.5}X2_{0.25}$** revealed a relatively sharp band between

Table 3 Results of the XRD experiments for the clustomesogens **Ter(*n*)·$Cs_{0.5}X_{0.25}$**

Ter(*n*)	Mesophase	Lattice spacing/Å	*d* spacing/Å exp. (calcd.)	Miller indices
Ter(14)·$Cs_{0.5}X1_{0.25}$	Col$_h$ *p6mm* (93 °C)	*a* = 38.86	33.65	(10)
			19.51 (19.43)	(11)
			17.09 (16.83)	(20)
			4.7	Halo
Ter(14)·$Cs_{0.5}X2_{0.25}$	Col$_h$ *p6mm* (140 °C)	*a* = 42.24	36.58	(10)
			21.00 (21.12)	(11)
			18.25 (18.29)	(20)
			4.3	Halo
Ter(16)·$Cs_{0.5}X1_{0.25}$	Col$_h$ *p6mm* (112 °C)	*a* = 42.38	36.70	(10)
			21.21 (21.19)	(11)
			18.51 (18.35)	(20)
			4.8	Halo
Ter(16)·$Cs_{0.5}X2_{0.25}$	Col$_h$ *p6mm* (131 °C)	*a* = 43.72	37.86	(10)
			21.59 (21.86)	(11)
			18.88 (18.93)	(20)
			4.3	Halo

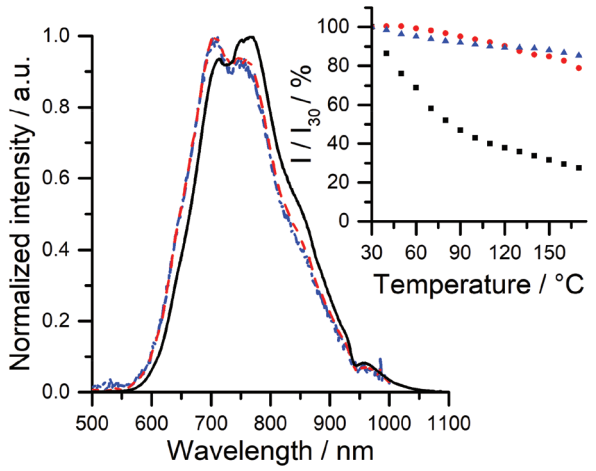

Fig. 7 Solid-state emission spectra measured at 30 °C for **Cs_2X1** (black line) and its complexes with **Ter(14)** (red dashes) and **Ter(16)** (blue dash-dot). Inset: Emission intensity evolution with the temperature for the same compounds: **Cs_2X1** (black squares), **Ter(14)** (red circles), **Ter(16)** (blue triangles).

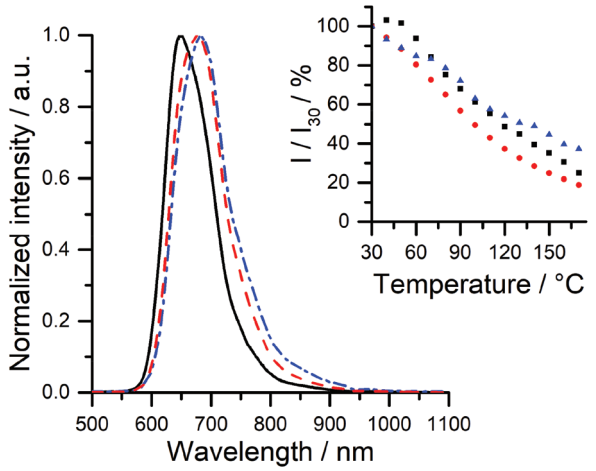

Fig. 8 Solid-state emission spectra measured at 30 °C for **Cs_2X2** (black line) and its complexes with **Ter(14)** (red dashes) and **Ter(16)** (blue dash-dot). Inset: Emission intensity evolution with the temperature for the same compounds: **Cs_2X2** (black squares), **Ter(14)** (red circles), and **Ter(16)** (blue triangles).

600 nm and 850 nm with the I_{max} at 678–684 nm (Fig. 8), similar to **Cs_2X2**.

For temperature-dependent emission measurements (inset, Fig. 7 and 8), the corresponding sample was heated to the isotropic state (170 °C). The spectra were taken upon cooling from the isotropic phase in steps of 10 K with a cooling rate of 1 K min^{-1}. As expected, an increase of the intensity could be observed for all clustomesogens **Ter(n)·$Cs_{0.5}X_{0.25}$** throughout the cooling process. As usual, when decreasing the temperature, the excited state is less affected by non-radiative deactivation, which in turn increases the luminescence intensity. However, native cluster salts and their respective complexes do not behave in the same way as depicted in Fig. 7 and 8 (insets). Remarkably, the complexes **Ter(n)·$Cs_{0.5}X1_{0.25}$** maintain up to 83% of the intensity at 170 °C compared to the I_0 at 30 °C, whereas the neat cluster salt $Cs_2[Mo_6Br_{14}]$ only shows 25% of its intensity at ambient temperature. For compounds **Ter(n)·$Cs_{0.5}X2_{0.25}$**, a greater loss of intensity was observed, leading to a maintained intensity of up to 37% at 170 °C. However, the corresponding neat cluster salt $Cs_2[Mo_6I_8(C_2F_5COO)_6]$ also shows at 170 °C only 25% of its intensity recorded at ambient temperature. It is well known that the environment of cluster anions (as counter-ions, crystal packing) influences greatly their relaxation processes and thus their abilities to emit.[32] As observed from ^{133}Cs MAS NMR experiments on **Ter(14)·$Cs_{0.5}X1_{0.25}$** and **Ter(14)·$Cs_{0.5}X2_{0.25}$** (see ESI Fig. S40†), interactions between cluster anions and Cs^+ seem negligible compared to crown ether Cs^+ interactions. Thus, cluster anions behave like isolated species in the liquid-crystalline phase, which in turn leads to enhanced emission thermal stability.

In addition, emission lifetime experiments and absolute quantum yield (AQY) measurements were performed on the **Cs_2X** salts (powder form) and thin-films for hybrids **Ter(n)·$Cs_{0.5}X_{0.25}$** (Table 4). Emission decay profiles, recorded at 23 °C, were fitted to a second order exponential decay and the goodness-of-fit was judged from the χ^2 values and their residual distribution. The calculated lifetimes for hybrids are lower than the respective **Cs_2X** lifetimes, ranging from 6.91 μs to 91.24 μs both for **Ter(14)·$Cs_{0.5}X2_{0.25}$**. These values are in line with previous lifetime component values determined for clustomesogens in the liquid-crystalline phase.[13b,33] The bi-exponential nature of the emission decay profile in the solid or LC state appears to be usual for such materials. It was already observed for powdered clusters or when clusters were embedded in other types of clustomesogens or polymers. The appearance of a second component in the emission decay might either arise from the cluster dual core emission abilities[32] or from excitation-energy transfer from the cluster to energy trap sites, such as surface defects.[34]

AQY measurements show that the ability of **Cs_2X1** to emit did not change upon complexation with crown ether ligands.[15] In contrast, hybrids based on the **Cs_2X2** salt and **Ter(14)** show higher AQY values than their neat **Cs_2X2** salt. We previously showed that the nature of cluster compound cations can have

Table 4 Solid state emission lifetime measurements of the hybrids at λ_{exc} = 375 nm and absolute quantum yield (AQY) measurements under a nitrogen atmosphere at λ_{exc} = 365 nm

Compound	τ_1/contribution	τ_2/contribution	AQY (N_2)
Ter(14)·$Cs_{0.5}X1_{0.25}$	15 μs/0.89	37 μs/0.11	15%
Ter(16)·$Cs_{0.5}X1_{0.25}$	19 μs/0.81	51 μs/0.19	15%
Ter(14)·$Cs_{0.5}X2_{0.25}$	7 μs/0.99	91 μs/0.01	52%
Ter(16)·$Cs_{0.5}X2_{0.25}$	9 μs/0.99	40 μs/0.01	37%
Cs_2X1	33 μs/0.50	89 μs/0.50	15%[a]
Cs_2X2	35 μs/0.48	116 μs/0.52	35%[a,b]

[a] Value calculated under an air atmosphere. [b] From ref. 19.

an important influence on their AQY. Therefore, it is not surprising, as observed for temperature-dependent emission studies, that a modification of the cluster anion environment influences its abilities to emit and thus its AQY.[13b,19]

Conclusion

To obtain luminescent lanthanide-free hybrid materials, novel liquid-crystalline tribenzo[18]crown-6 *o*-terphenyl compounds **Ter(*n*)** and the corresponding triphenylene compounds **Tri(*n*)** were prepared and used as ligands for complexation with inorganic cluster compounds $Cs_2[Mo_6Br_{14}]$ and $Cs_2[Mo_6I_8(C_2F_5COO)_6]$. However, *o*-terphenyl derivatives **Ter(*n*)** provided the desired hybrid materials **Ter(*n*)·Cs$_{0.5}$X$_{0.25}$** (n = 14, 16) (**X1** = $[Mo_6Br_{14}]^{2-}$; **X2** = $[Mo_6I_8(C_2F_5COO)_6]^{2-}$), as shown by ^{133}Cs MAS NMR spectroscopy, and the respective triphenylenes **Tri(*n*)** led to decomposition.

On comparing the mesomorphic properties of metal-free tribenzo[18]crown-6 *o*-terphenyls **Ter(*n*)** with the corresponding tribenzo[18]crown-6 triphenylenes, the **Tri(*n*)** compounds (see ESI pp. S5–S7†) showed higher melting and clearing temperatures, while the phase widths remained mostly unaffected. In contrast, in the hybrid materials **Ter(14)·Cs$_{0.5}$X$_{0.25}$** and **Ter(16)·Cs$_{0.5}$X$_{0.25}$** containing the cluster anions $[Mo_6Br_{14}]^{2-}$ and $[Mo_6I_8(C_2F_5COO)_6]^{2-}$, the mesophase stability was significantly increased, with higher clearing and decreased melting temperatures. This led to room-temperature clustomesogens with the Col$_h$ phase that persisted up to 147 °C for **Ter(14)·Cs$_{0.5}$[Mo$_6$Br$_{14}$]$_{0.25}$** and up to 159 °C for **Ter(14)·Cs$_{0.5}$[Mo$_6$I$_8$(C$_2$F$_5$COO)$_6$]$_{0.25}$**, respectively, compared to 98 °C for the parent crown **Ter(14)**. The stabilizing effect was even more pronounced for the mixed iodo anion $[Mo_6I_8(C_2F_5COO)_6]^{2-}$ as compared to the bromo anion $[Mo_6Br_{14}]^{2-}$. This outcome can be rationalized by a hexagonal columnar packing, in which the cluster anions are embedded by the *o*-terphenyl crowns, whereas the Cs^+ counter-cations are sandwiched between the centers of two crowns. The complexation of the crown ethers with the cluster salts had an additional effect on the lattice parameters. XRD studies revealed an *a* value of 45.06 Å for the metal-free *o*-terphenyl crown **Ter(14)**. Upon complexation with the cluster salts, the *a* values decreased to 38.86 Å and 42.24 Å for the clustomesogens **Ter(14)·Cs$_{0.5}$[Mo$_6$Br$_{14}$]$_{0.25}$** and **Ter(14)·Cs$_{0.5}$[Mo$_6$I$_8$(C$_2$F$_5$COO)$_6$]$_{0.25}$**, respectively, with the former value being even smaller than the lattice parameter of the metal-free triphenylene **Tri(14)**. Presumably, electrostatic interactions between the Cs^+ crown sandwich and the cluster anion lead to a 2D contraction of the hexagonal columnar lattice.

The emission properties of the metal clusters were also affected by the complexation of Cs^+ cations within the **Ter(*n*)** crown ether and were preserved within the mesophase. The interactions with **Ter(*n*)** ligands led to a lower deactivation process during heating, which resulted in brighter luminescence even at high temperatures. The calculated lifetime values are in line with the already reported values for clustomesogens and reflect the phosphorescence abilities of the anionic cluster units.

These hybrid materials represent rare examples of anisometric emissive species that are introduced in a columnar liquid-crystalline phase. Their versatility and ease of synthesis should allow the realization of a library of hybrid compounds in the near future, allowing a better understanding of their synergistic effects both on the liquid-crystalline phase stabilization and emission properties.

Conflicts of interest

There are no conflicts to declare.

Acknowledgements

Generous financial support by the Deutsche Akademische Austauschdienst (PPP Procope program PLISE) as well as l'Agence Nationale de la Recherche (ANR Clustomesogen ANR-13-BS07-0003-01) and Fondation Langlois, the Ministerium für Wissenschaft, Forschung und Kunst des Landes Baden-Württemberg, the Bundesministerium für Bildung und Forschung (shared instrumentation grant # 01 RI 05177), the Carl-Schneider-Stiftung Aalen (shared instrumentation grant) and the Fonds der Chemischen Industrie (Kekulé PhD fellowship for S. B.) is gratefully acknowledged.

Notes and references

1 Reviews: (*a*) J. M. Lehn, *Chem. Scr.*, 1988, **28**, 237–262; (*b*) D. J. Cram, *Chem. Scr.*, 1988, **28**, 263–274; (*c*) C. J. Pedersen, *Chem. Scr.*, 1988, **28**, 229–235.

2 Reviews: (*a*) J. P. Sauvage, *Angew. Chem., Int. Ed.*, 2017, **56**, 11080–11093; (*b*) J. F. Stoddart, *Angew. Chem., Int. Ed.*, 2017, **56**, 11094–11125; (*c*) B. L. Feringa, *Angew. Chem., Int. Ed.*, 2017, **56**, 11060–11079.

3 Reviews: (*a*) S. Laschat, A. Baro, T. Wöhrle and J. Kirres, *Liq. Cryst. Today*, 2016, **25**, 48–60; (*b*) M. Kaller, A. Baro and S. Laschat in *Handbook of Liquid Crystals*, ed. J. W. Goodby, P. J. Collings, T. Kato, C. Tschierske, H. Gleeson and P. Raynes, Wiley-VCH, Weinheim, 2nd edn, 2014, vol. 6, pp. 335–376; (*c*) M. Kaller and S. Laschat, *Top. Curr. Chem.*, 2012, **318**, 109–192; (*d*) J. W. Goodby, G. H. Mehl, I. M. Saez, R. P. Tuffin, G. Mackenzie, R. Auzély-Velty, T. Benvegnu and D. Plusquellec, *Chem. Commun.*, 1998, 2057–2070.

4 Recent examples: (*a*) K. Bader, M. M. Neidhardt, T. Wöhrle, R. Forschner, A. Baro, F. Giesselmann and S. Laschat, *Soft Matter*, 2017, **13**, 8379–8391; (*b*) J. Kirres, F. Knecht, P. Seubert, A. Baro and S. Laschat, *ChemPhysChem*, 2016, **17**, 1159–1165; (*c*) C. W. Ong, C. Q. Yan, M.-C. Yeh and M.-C. Tzeng, *Mol. Cryst. Liq. Cryst.*, 2015, **610**, 249–254; (*d*) Y. Ma, T. Marszalek, Z. Yuan, R. Stangenberg, W. Pisula, L. Chen and K. Müllen, *Chem. – Asian J.*, 2015, **10**, 139–143;

(*e*) T. Wöhrle, J. Kirres, M. Kaller, M. Mansueto, S. Tussetschläger and S. Laschat, *J. Org. Chem.*, 2014, **79**, 10143–10152; (*f*) H. Guo, J. Ye and F. Yang, *Liq. Cryst.*, 2014, **41**, 946–952; (*g*) T. Basova, F. Latteyer, D. Atilla, A. Hassan, V. Ahsen, H. Peisert and T. Chassè, *Thin Solid Films*, 2010, **518**, 5745–5752; (*h*) A. Mori, E. Yamamoto, K. Kubo, S. Ujiie, U. Baumeister and C. Tschierske, *Liq. Cryst.*, 2010, **37**, 1059–1065; (*i*) R. Ziessel, F. Camerel and B. Donnio, *Chem. Rec.*, 2009, **9**, 1–23; (*j*) X. Zhou, S. Kang, S. Kumar and Q. Li, *Liq. Cryst.*, 2009, **36**, 269–274.

5 Recent examples: (*a*) P. Thuery, Y. Atoini and J. Harrowfield, *Cryst. Growth Des.*, 2018, **18**, 3167–3177; (*b*) R. Donamaría, V. Lippolis, J. M. López-de-Luzuriaga, M. Monge, M. Nieddu and M. E. Olmos, *Inorg. Chem.*, 2017, **56**, 12551–12563; (*c*) M. Al Hareri, Z. Ras Ali, J. Regier, E. L. Gavey, L. D. Carlos, R. A. S. Ferreira and M. Pilkington, *Inorg. Chem.*, 2017, **56**, 7344–7353; (*d*) F. Gao, F.-L. Yang, X. Feng, H. Xu, W. Sun, H. Liu and X.-L. Li, *Dalton Trans.*, 2017, **46**, 1317–1323; (*e*) A. J. Blake, R. Donamaría, V. Lippolis, J. M. López-de-Luzuriaga, E. Manso, M. Monge and E. M. Olmos, *Inorg. Chem.*, 2014, **53**, 10471–10484; (*f*) H. Lin, M. E. Cinar and M. Schmittel, *Dalton Trans.*, 2010, **39**, 5130–5138.

6 For a mechano-responsive luminescent material based on discotic crown ether doped with organic fluorophores see: B. Zhang, C. Hsu, Z. Yu, S. Yang and E. Chen, *Chem. Commun.*, 2013, **49**, 8872–8874.

7 J. R. Long, L. S. McCarty and R. H. Holm, *J. Am. Chem. Soc.*, 1996, **118**, 4603–4616.

8 (*a*) M. N. Sokolov, M. A. Mihailov, E. V. Peresypkina, K. A. Brylev, N. Kitamura and V. P. Fedin, *Dalton Trans.*, 2011, **40**, 6375–6377; (*b*) A. W. Maverick, J. S. Najdzionek, D. MacKenzie, D. G. Nocera and H. B. Gray, *J. Am. Chem. Soc.*, 1983, **105**, 1878–1882.

9 J. C. Sheldon, *J. Chem. Soc.*, 1960, 1007.

10 M. Robin, N. Dumait, M. Amela-Cortes, C. Roiland, M. Harnois, E. Jacques, H. Folliot and Y. Molard, *Chem. – Eur. J.*, 2018, **24**, 4825–4829.

11 Y. Molard, *Acc. Chem. Res.*, 2016, **49**, 1514–1523.

12 Review: D. Pucci and B. Donnio, *Handbook of Liquid Crystals*, ed. J. W. Goodby, P. J. Collings, T. Kato, C. Tschierske, H. Gleeson and P. Raynes, Wiley-VCH, Weinheim, 2nd edn, 2014, vol. 5, 175–241.

13 (*a*) K. Guy, P. Ehni, S. Paofai, R. Forschner, C. Roiland, M. Amela-Cortes, S. Cordier, S. Laschat and Y. Molard, *Angew. Chem., Int. Ed.*, 2018, **57**(36), 11692–11696; (*b*) M. Prévôt, M. Amela-Cortes, S. K. Manna, S. Cordier, T. Roisnel, H. Folliot, L. Dupont and Y. Molard, *J. Mater. Chem. C*, 2015, **3**, 5152–5161; (*c*) Y. Wang, X. Wang, X. Zhang, N. Xia, B. Liu, J. Yang, W. Yu, M. Hu, M. Yang and W. Wang, *Chem. – Eur. J.*, 2010, **16**, 12545–12548; (*d*) Y. Yang, Y. Wang, H. Li, W. Li and L. Wu, *Chem. – Eur. J.*, 2010, **16**, 8062–8071; (*e*) X. Lin, W. Li, J. Zhang, H. Sun, Y. Yan and L. Wu, *Langmuir*, 2010, **26**, 13201–13209; (*f*) A. S. Mocanu, M. Amela-Cortes, Y. Molard, V. Cîrcu and S. Cordier, *Chem. Commun.*, 2011, **47**, 2056–2058; (*g*) D.-L. Long, R. Tsunashima and L. Cronin, *Angew. Chem., Int. Ed.*, 2010, **49**, 1736–1758; (*h*) A. Dolbecq, E. Dumas, C. R. Mayer and P. Mialane, *Chem. Rev.*, 2010, **110**, 6009–6048; (*i*) C. Cordovilla, S. Coco, P. Espinet and B. Donnio, *J. Am. Chem. Soc.*, 2010, **132**, 1424–1431; (*j*) T. B. Jensen, E. Terazzi, K.-L. Buchwalder, L. Guénée, H. Nozary, K. Schenk, B. Heinrich, B. Donnio, D. Guillon and C. Piguet, *Inorg. Chem.*, 2010, **49**, 8601–8619.

14 For recent related examples see: (*a*) T. Mori, A. Sharma and T. Hegmann, *ACS Nano*, 2016, **10**, 1552–1564; (*b*) T. T. Nguyen, T. A. Le Nguyen and R. Deschenaux, *J. Porphyrins Phthalocyanines*, 2016, **20**, 1060–1064; (*c*) M. L. Rahman, T. K. Biswas, S. M. Sarkar, M. M. Yusoff, A. R. Yuvaraj and S. Kumar, *J. Colloid Interface Sci.*, 2016, **478**, 384–393; (*d*) D. Jishkariani, B. T. Diroll, M. Cargnello, D. R. Klein, L. A. Hough, C. B. Murray and B. Donnio, *J. Am. Chem. Soc.*, 2015, **137**, 10728–10734; (*e*) W. Li and L. Wu, *Polym. Int.*, 2014, **63**, 1750–1764.

15 S. K. Nayak, M. Amela-Cortes, C. Roiland, S. Cordier and Y. Molard, *Chem. Commun.*, 2015, **51**, 3774–3777.

16 S. K. Nayak, M. Amela-Cortes, M. M. Neidhardt, S. Beardsworth, J. Kirres, M. Mansueto, S. Cordier, S. Laschat and Y. Molard, *Chem. Commun.*, 2016, **52**, 3127–3130.

17 N. Steinke, W. Frey, A. Baro, S. Laschat, C. Drees, M. Nimtz, C. Hägele and F. Giesselmann, *Chem. – Eur. J.*, 2006, **12**, 1026–1035.

18 K. Kirakci, S. Cordier and C. Perrin, *Z. Anorg. Allg. Chem.*, 2005, **631**, 411–416.

19 M. Amela-Cortes, Y. Molard, S. Paofai, A. Desert, J.-L. Duvail, N. G. Naumov and S. Cordier, *Dalton Trans.*, 2016, **45**, 237–245.

20 C. J. Pedersen, *J. Am. Chem. Soc.*, 1967, **89**, 7017–7036.

21 E. Weber, *Chem. Ber.*, 1985, 4439–4452.

22 (*a*) C. J. Pedersen, *J. Am. Chem. Soc.*, 1970, **92**, 386–391; (*b*) T. Akutagawa, K. Shitagami, M. Aonuma, S.-I. Noro and T. Nakamura, *Inorg. Chem.*, 2009, **48**, 4454–4461.

23 H.-R. Yu, J.-Q. Hu, X.-H. Lu, X.-J. Ju, Z. Liu, R. Xie, W. Wang and L.-Y. Chu, *J. Phys. Chem. B*, 2015, **119**, 1696–1705.

24 I. A. Weinstock, K. E. Hammel, M. A. Moen, L. L. Landucci, S. Ralph, C. E. Sullivan and R. S. Reiner, *Holzforschung*, 1998, **52**, 311–318.

25 R. S. Assary, A. C. Atesin, Z. Li, L. A. Curtiss and T. J. Marks, *ACS Catal.*, 2013, **3**, 1908–1914.

26 E. Quaranta, *Appl. Catal., B*, 2017, **206**, 233–241.

27 J. M. Keith, *Tetrahedron Lett.*, 2004, **45**, 2739–2742.

28 R. Litlabo, H. S. Lee, M. Niemeyer, K. W. Tornroos and R. Anwander, *Dalton Trans.*, 2010, **39**, 6815–6825.

29 (*a*) S.-i. Kawano, Y. Ishida and K. Tanaka, *J. Am. Chem. Soc.*, 2015, **137**, 2295–2302; (*b*) X. Li, B. Li, L. Chen, J. Hu, C. Wen, Q. Zheng, L. Wu, H. Zeng, B. Gong and L. Yuan, *Angew. Chem., Int. Ed.*, 2015, **54**, 11147–11152.

30 S. Shinkai, T. Nishi, A. Ikeda, T. Matsuda, K. Shimamoto and O. Manabe, *J. Chem. Soc., Chem. Commun.*, 1990, **44**, 303–304.

31 M. Kaller, P. Staffeld, R. Haug, W. Frey, F. Giesselmann and S. Laschat, *Liq. Cryst.*, 2011, **38**, 531–553.
32 K. Costuas, A. Garreau, A. Bulou, B. Fontaine, J. Cuny, R. Gautier, M. Mortier, Y. Molard, J.-L. Duvail, E. Faulques and S. Cordier, *Phys. Chem. Chem. Phys.*, 2015, **17**, 28574–28585.
33 M. Prévôt, M. Amela-Cortes, S. K. Manna, R. Lefort, S. Cordier, H. Folliot, L. Dupont and Y. Molard, *Adv. Funct. Mater.*, 2015, **25**, 4966–4975.
34 E. Sakuda, K. Tsuge, Y. Sasaki and N. Kitamura, *J. Phys. Chem. B*, 2005, **109**, 22326–22331.